Materials Today Communications 15 (2018) 70–80

Contents lists available at ScienceDirect

Materials Today Communications

journal homepage: www.elsevier.com/locate/mtcomm

Electromagnetic interference shielding effectiveness of ABS carbon-based composites manufactured via fused deposition modelling

D.P. Schmitz[a], L.G. Ecco[a,b,*], S. Dul[b], E.C.L. Pereira[c], B.G. Soares[c], G.M.O. Barra[a], A. Pegoretti[b]

[a] Department of Mechanical Engineering, Federal University of Santa Catarina – UFSC, Florianópolis, SC, Brazil
[b] Department of Industrial Engineering, University of Trento, Trento, Italy
[c] Department of Metallurgic and Materials Engineering, Federal University of Rio de Janeiro, Rio de Janeiro, RJ, Brazil

ARTICLE INFO

Keywords:
Nanocomposites
Fused deposition modelling
Electromagnetic interference shielding

ABSTRACT

3-D printed samples based on acrylonitrile-butadiene-styrene (ABS) loaded with multi-walled carbon nanotubes (CNT), carbon black (CB) and a 50:50 hybrid combination (CNT/CB) were manufactured via fused deposition modelling (FDM). The electromagnetic interference shielding efficiency (EMI SE) of resulting FDM specimens was assessed. Different amounts of CNT, CB and CNT/CB were dispersed in an ABS matrix by melt compounding using an internal mixer. On the basis of the rheological behavior a weight fraction of 3% was selected for the filaments production. The filaments were prepared using a twin-screw extruder and used to feed a commercial FDM machine for 3-D printed specimen's preparation along three different growing directions. The electrical conductivity, the EMI SE and the mechanical properties of the resulting extruded filaments, as well as the 3-D printed specimens, were measured and, they are discussed in terms of the type of filler and growing directions. In general, the conductivity, EMI SE and mechanical properties of 3D printed parts were markedly dependent on the growing direction. Through the experimental findings of this work, an appropriate choice of a polymer nanocomposite formulation alongside the 3-D printing parameters could lead to components manufactured via FDM with optimized EMI SE and mechanical properties.

1. Introduction

The technologies of preparing three-dimensional components by additive manufacturing (AM) are rapidly expanding. In the last years, the expiration of early patents related to AM technologies made available devices, machinery and materials to industry, academy and general public causing a significant grown in the global sales of AM technologies. Recent advances in AM techniques allow a significant time and cost reduction in the production of complex components. Thus, AM is becoming a competitive approach to be used in various fields such as dentistry, mechanical engineering, and architecture [1–5].

Amongst the AM processes, fused deposition modelling (FDM) appears as an emerging technology and represents one of the most common techniques for rapid prototyping of polymeric parts. In this technique, the component is built layer by layer from filament extrusion and deposition on a plate. FDM is relatively cheaper than other AM technologies. In fact, the machinery is relatively less expensive and the feedstock filament (raw material) can be easily supplied or even produced [6,7]. Moreover, open source software's to design and control the process are available. The most common thermoplastic polymers employed in FDM are poly(acrylonitrile-co-butadiene-co-styrene) (ABS) and poly(lactic acid) (PLA) [8–10]. Latest advances in this technology have also permitted to use high-performance engineering polymers such as poly(ether ether ketone) (PEEK) [11,12]. It is important to highlight that the properties of the polymeric components fabricated via FDM are dependent on the growing direction. Anisotropy of the solid parts produced via FDM has been demonstrated in mechanical [13], dynamic-mechanical [6], electrical conductivity [14] and thermal conductivity [15] properties.

In view of such inherently characteristic of the process, a viable strategy to add some functionalities to the components fabricated via FDM is to develop polymer composites filaments [16,17]. In this framework, electrically conductive polymer nanocomposites are an important example. The addition of carbon-based nanofillers, such as carbon black (CB) and carbon nanotubes (CNT), modify the complex permittivity of the polymer raising their electrical conductivity. Likewise, the modifications in the complex permittivity caused by the addition of these fillers allow electrically conductive polymer nanocomposites to be employed as shielding materials for the electromagnetic radiation [18]. Electronic devices, such as weather

* Corresponding author at: Department of Mechanical Engineering, Federal University of Santa Catarina – UFSC, Florianópolis, SC, Brazil.
E-mail address: luiz.ecco@labmat.ufsc.br (L.G. Ecco).

https://doi.org/10.1016/j.mtcomm.2018.02.034
Received 17 February 2018; Accepted 26 February 2018
Available online 27 February 2018
2352-4928/

radars, portable computers, mobile phones, transmitters, etc., irradiate electromagnetic signals while in service and, once the emitted signals affect its own or the operation of other devices electromagnetic interference (EMI) may happen. Thus in present days, there is a crucial need for developing effective and practical EMI shielding materials [18–20].

Electrically conductive polymer nanocomposites envisioned for EMI shielding applications have been investigated in the last years [21–23]. The use of carbon-based over the more traditional metallic fillers render these polymer composites advantageous since weight reduction and higher corrosion resistance are achieved [24]. Both solvent cast [25] and melt mixing followed by compression molding [26] are main methods used in the preparation of the formulations developed for EMI shielding applications. Despite the fact that many works report the use of carbonaceous based polymer nanocomposites for EMI shielding applications, to the best of our knowledge the preparation of electrically conductive components targeted to EMI shielding effectiveness via fused deposition modelling remains a subject to be investigated. Preparing conductive filament, i.e. extruding highly concentrated carbon-based polymer composites, is a challenging task. Recently, the fabrication of electrically conductive polymer composites by means of FDM has been reported. It has been verified that highly filled composites showed high viscosity in the molten state [14,27]. The printing nozzle experienced obstruction and due to processing limitations formulations at a weight fraction higher than 4 wt.% could not be processed [6].

With respect to the above considerations, this work reports the preparation of electrically conductive and efficient EMI shielding ABS-carbonaceous based nanocomposites specimens via FDM. Initially, an investigation on the rheological behavior of the ABS composites is made for the selection of the formulations to be processed via FDM. The feedstock filaments for FDM were prepared at a fixed filler weight fraction of 3 wt.% consisting of carbon nanotube (CNT), carbon black (CB) as well as hybrid formulation (both CNT and CB). In order to verify the effect of the printing pattern of FDM, the solid components were built along three different growing directions and the electromagnetic interference shielding effectiveness of the specimens was assessed in the X-band frequency range.

2. Experimental

2.1. Materials

An acrylonitrile–butadiene–styrene (ABS) copolymer was supplied in pellets form by Sabic, Brazil under the trade name of Cycolac™ Resin MG47. For the preparation of the polymer nanocomposites the following carbonaceous filler were used: multi-walled carbon nanotubes, trade name Nanocyl™ NC7000 provided by Nanocyl S.A, Belgium; carbon black trade name PRINTEX XE 2-B, purchased from Orion Engineered Carbon, US. The nanocomposites were prepared at a fixed filler weight fraction of 3 wt.% of each filler as well as hybrid (50:50), as detailed in Table 1.

2.2. Composites preparation and FDM manufacturing

2.2.1. Compounding

Before processing the ABS pellets and the carbonaceous fillers were vacuum dried overnight at 60 °C. Neat ABS, as well as ABS/nanocomposites, were prepared using an internal mixer (Thermo Scientific Haake™, Polylab™ Rheomix) with mixing chamber capacity of 75 g and counter-rotating rotors. The temperature in the mixing chamber was 230 °C, the rotors speed set at 60 rpm for a mixing time of 15 min. To properly feed the extruder, the resulting materials were reduced to millimeter-sized particles using a low-speed granulator (Piovan, model: RN 166).

Table 1
Nanocomposites formulations used for the preparation of FDM specimens.

Label	Filler	Composite formulation (wt.%)
ABS	–	ABS (100)
ABS/CNT	MWCNT	ABS (97)/CNT (3)
ABS/CB	Carbon black	ABS (97)/CB (3)
ABS/HYB	MWCNT + Carbon black	ABS (97)/CNT (1.5)/CB (1.5)

2.2.2. Filament preparation

Before filament extrusion, the granulated materials were vacuum dried overnight at 60 °C. Neat ABS and the nanocomposites filaments were prepared using a Thermo Haake PTW16 intermeshing co-rotating twin-screw extruder (screw diameter = 16 mm; L/D ratio = 25; rod die diameter 1.80 mm). The processing temperature of feeding zone (Zone 1) to rod die (Zone 5) increased from 150, 210, 215, 215 and 220 °C, respectively. The screw rotation speed was fixed at 10 rpm, and the collection rate was regulated in order to obtain a final diameter of the extruded filaments of 1.75 ± 0.10 mm. Two parameters of the process, the pressure at the die and torque were constantly recorded during the production of the filaments. As shown in Fig. 1, after 20 min of extrusion time the monitored parameters assumed plateau values. It is also interesting to observe how both parameters assume lower values for the neat ABS and higher values when CB is added and even higher values when CNT and hybrid systems are considered.

2.2.3. Preparation of the specimens via FDM for EMI SE

Before FDM manufacturing the extruded filaments were vacuum dried overnight at 60 °C. The specimens were produced using a Sharebot Next Generation machine (Sharebot NG, Nibionno, Italy). The manufacturing process was controlled and designed using the open source software *Slic3r*. The following printing parameters were selected and maintained constant for all the composites formulations: object infill 100%; deposition rate of 40 mm/s; nozzle diameter 0.4 mm; layer height 0.20 mm; nozzle temperature 250 °C; printing platform temperature 110 °C. The layer height and the object infill are the diameter of the deposited filament and the percentage of infill of the space inside the solid layers and the perimeters, respectively.

For EMI SE analysis, the specimens were designed into a square shape with a side of 45 mm and a thickness of 2 mm, and they were built-up along three different growing directions named perpendicular concentric (PC), horizontal alternate (H45) and horizontal concentric (HC), as shown in the schematic representation given in Fig. 2. The dimensions have been specifically defined on the basis of the EMI SE tests specifications.

In the PC and HC growing directions, the layers were built along concentric lines from the outside towards interior having all the layers being deposited as identical as the previous; in the H45, the layers were built alternating the succeeding deposited layer by an inclination of 90° with respect to the previous wherein the very first layer had 45° with respect to the origin. The estimated total filament length and weight used in the manufacture of the specimens as a function of growing direction are given in Table 2. In addition, Table 2 shows the average weight of the solid components. Accordingly, the specimens built along PC growing direction were found approximately 4045 g lighter than those built along HC and H45 directions independent on the composite formulation.

2.2.4. Preparation of the specimens via FDM for quasi-static tensile test

For quasi-static tensile test, the 3-D printed samples were designed into the dumbbell geometry using the same growing directions: HC, H45 and PC, in accordance to ISO 527 type 5A, i.e. a gage length of 25 mm, a width of 4 mm and a thickness of 2 mm, as shown in Fig. 3.

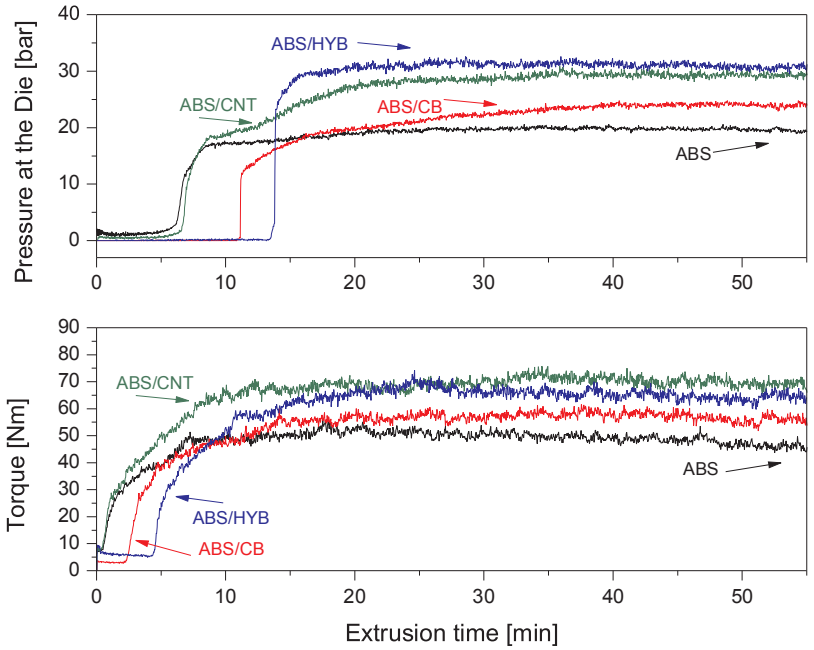

Fig. 1. Evolution of pressure at the die (upper graph) and torque (lower graph) during the filament extrusion for neat ABS and carbonaceous-based composites.

2.3. Testing

2.3.1. Density measurements

The density of carbon-based fillers was measured by means of gas helium pycnometry technique using a Micromeritics Accupyc 1330 helium Pycnometer. The measures were performed using a testing chamber of 3.5 cm^3 at 23 °C. A known mass of each of the carbonaceous filler was added into the testing chamber and approximately 300 acquisitions were conducted. The values reported representing the average of the last 100 measures wherein constant values ware acquired.

Density measurements were conducted for the extruded filaments using solvent ethanol-water (a concentration of 96 wt.% and density of 0.817 g/cm^3) at room temperature, and at least three replicated specimens for each sample according to the standard ASTM D792-13 and the density is calculated through Eq. (1).

$$\rho_{exp} = \frac{m_{air} \times \rho_{ethanol}}{m_{air} - m_{ethanol}} \quad (1)$$

where m_{air} and $m_{ethanol}$ are the mass of samples in air and ethanol respectively. In order to compare the experimental results, theoretical density of composites was predicted based on the rule of mixtures, as presented in Eq. (2).

$$\rho_{th} = \rho_m \times V_m + \rho_f \times V_f \quad (2)$$

where ρ_{th}, ρ_m, ρ_f are the theoretical density of the composite, the neat matrix, and the nanoparticles respectively. V_m and V_f stand for the volume fraction of the matrix and the nanofillers, respectively. Lastly, the content of voids in nanocomposites was evaluated following Eq. (3):

$$V_V = \frac{\rho_{exp} - \rho_{th}}{\rho_{th}} \quad (3)$$

The composites were prepared at a weight concentration of 3%, thus the conversion from weight to volume concentration (vol.%) was calculated according to Eq. (4):

$$vol.\ \% = \frac{\frac{fw}{\rho f}}{\frac{fw}{\rho f} + \frac{(1-fw)}{\rho m}} \cdot 100(\%) \quad (4)$$

where ρ_f and ρ_m are the densities of the additives and the matrix, respectively, and f_w is the weight fraction of the additives, equal to 0.03. In particular, Eq. (4) was adjusted to Eq. (5) for calculating the volume concentration of the hybrid composite, as follows:

$$\text{vol.}\% = \frac{\frac{(fw1 \times \rho 2) + (fw2 \times \rho 1)}{\rho 1 \times \rho 2}}{\frac{(fw1 \times \rho 2) + (fw2 \times \rho 1)}{\rho 1 \times \rho 2} + \frac{(1 - fw1 - fw2)}{\rho m}} \cdot 100(\%) \quad (5)$$

Where, $\rho_1$and ρ_2 are the densities of either MWCNT or CB whereas *fw1* and *fw2* are the weight fraction of the additives. ρ_m is the density of the matrix.

2.3.2. Scanning electron microscopy

Morphology of nanocomposites was studied by using a JEOL JSM-6701 scanning electron microscopy (SEM). For cross-sectional analysis of the nanocomposites, FDM specimens were fractured in liquid nitrogen, gold coated and observed at an acceleration voltage of 10 kV.

2.3.3. Rheological analysis

Rheological properties of neat ABS and the nanocomposites were evaluated using an oscillatory rheometer, model Hybrid Discovery HR1 from TA Instrument Inc., with parallel plate geometry (25 mm). The analysis was performed at a temperature of 230 °C and range frequency of 0.01–100 Hz with a 0.5% deformation, in the linear viscoelastic regime.

2.3.4. Electrical conductivity measurements

The electrical conductivity (σ) in the direct current regime of resulting composites was assessed both on the feedstock filaments for fused deposition modelling as well as on the specimens manufactured via FDM. The measurements were conducted on a portion of the filament having 1.75 mm diameter and 20 mm long, by means of the four-probe technique. The experimental arrangement consisted in applying known currents at the external probes and measuring the voltage difference, i.e. potential drop, generated between the two internal probes. It was used a Metrohm-Autolab potentiostat, model PGSTAT302N operated in galvanostat mode. Measurements were carried out at room temperature. The resultant values of potential and current were inputted in the formula given in Eq. (6) to calculate the electrical conductivity,

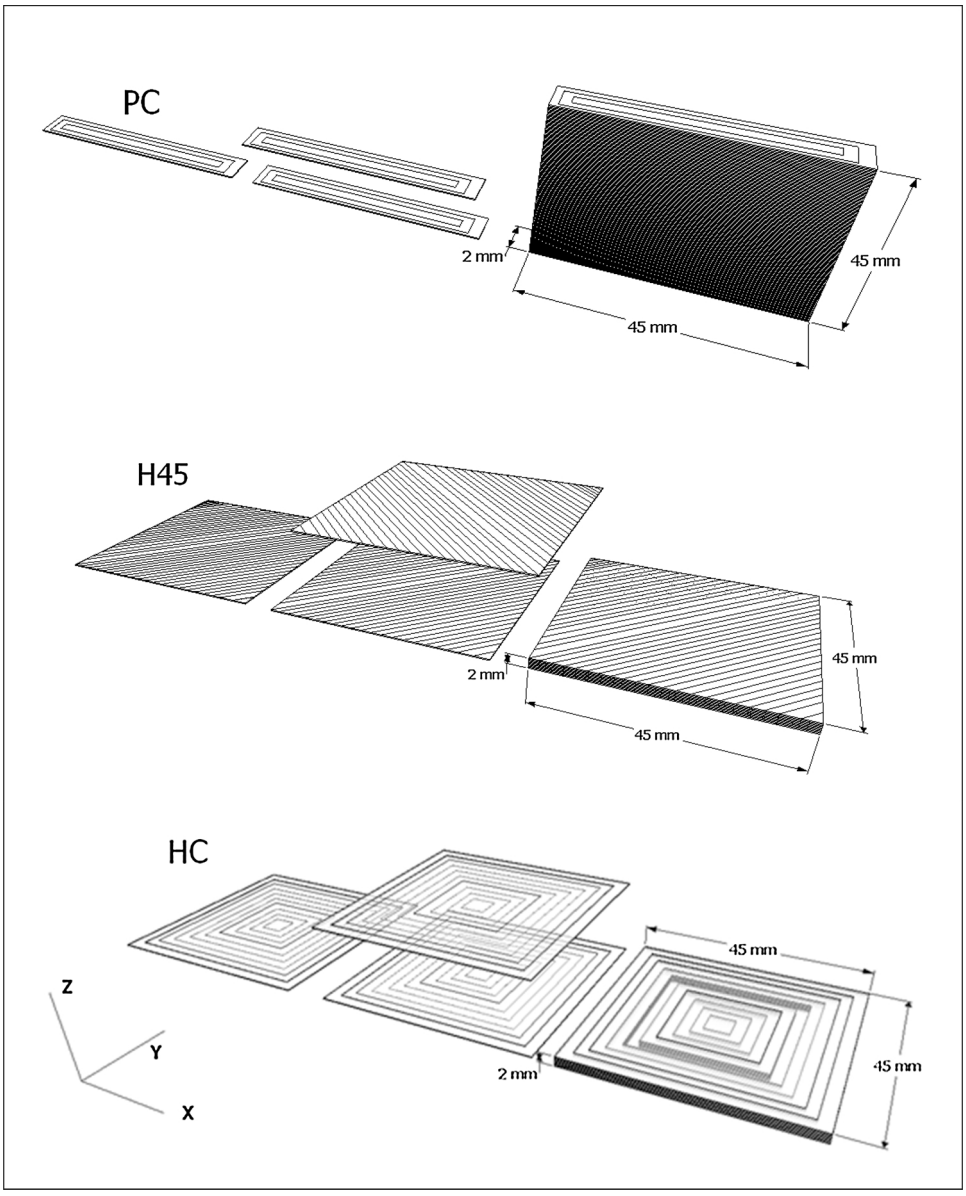

Fig. 2. Schematic representation of the specimens built along the three growing directions. For each growing direction from the left to the right: first deposited layer, representation of the second layer and, the resulting solid component with proper dimensions.

Table 2
General information on the manufacturing process for building the specimens along the growing directions.

FDM processing		Growing direction		
		PC	HC	H45
Estimated total filament length[a] [mm]		1867.68	2338.56	2388.39
Estimated total filament weight[a] [g]		4.41	5.52	5.64
Average weight of the FDM specimens [g]	ABS	3.62 ± 0.01	4.04 ± 0.02	4.03 ± 0.03
	ABS/CNT	3.65 ± 0.02	4.06 ± 0.01	4.06 ± 0.02
	ABS/CB	3.64 ± 0.03	4.09 ± 0.02	4.09 ± 0.01
	ABS/HYB	3.64 ± 0.02	4.10 ± 0.02	4.09 ± 0.01

[a] Values estimated by Slic3r software.

$$\sigma = \frac{i \times \ln 2}{V \times \pi \times t \times 10^{-1}} \quad (6)$$

where: i is the applied current (Ampere), V is the voltage (Volts) and t is the sample diameter (cm).

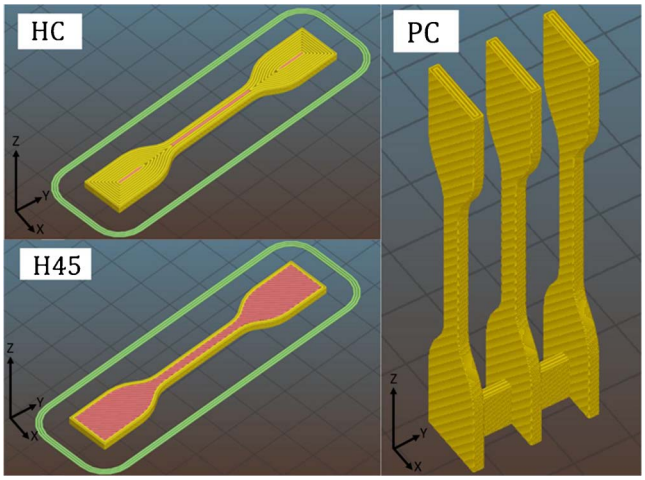

Fig. 3. Schematic of 3D-printed dumbbell: (a) horizontal concentric (HC); (b) horizontal 45°angle (H45) and (c) perpendicular concentric (PC) [17].

Table 3
Density of the carbonaceous fillers. Polymer nanocomposites volume fraction, density and voids fraction.

Filler	Density – He pycnometry (g/cm^3)	Polymer nanocomposites	Volume fraction (vol.%)	Density – ASTM D792-13 (g/cm^3)	Density – Rule of mixtures (g/cm^3)	Voids fraction (%)
MWCNT	2.287 ± 0.099	ABS	–	1.034 ± 0.001	1.040	–
		ABS/CNT	1.383	1.049 ± 0.003	1.057	0.77
CB	2.389 ± 0.066	ABS/CB	1.325	1.048 ± 0.003	1.058	0.92
		ABS/HYB	1.354	1.051 ± 0.002	1.057	0.61

The electrical volume conductivity measurements of the samples prepared via FDM were carried out using a Keithley 8009 resistivity test fixture. The experimental arrangement consisted in placing the specimens between two terminals, applying a voltage potential across opposite sides of the specimen and measuring the resultant current through the sample. Measurements were carried out at room temperature. The volume conductivity stated by ASTM D257 is therefore calculated according to Eq. (7), where: t is the average thickness of the sample (cm), A is the effective area (cm^2) of the guarded electrode and R is the volume resistance (Ohm).

$$\sigma = \frac{t}{A} \times \frac{1}{R} \tag{7}$$

2.3.5. Electromagnetic interference measurements

EMI SE was evaluated in the frequency between 8.2–12.4 GHz, corresponding to the X-band microwave range using an Agilent Technology PNA series network analyzer (N5230C Agilent PNA-L) with a rectangular waveguide.

The experimental arrangement consisted in positioning the specimens at the sample holder placed between the two waveguide ports of the network analyzer. The instrumentation applies an incident electromagnetic wave of known power over the specific frequency range and collects both, the transmitted and the reflected waves between the two ports. In effect, it measures the magnitude and phase of the scattering parameters (S_{11} and S_{21}), known as S-parameters, of the specimen localized between the two ports. S_{11} corresponds to the power released from and returned to port 1 whereas S_{21} to those released from port 2 and collect at port 1. The EMI SE is defined as the ability of a conductive material to attenuate the electromagnetic waves. The attenuation is expressed in decibels (dB) and can be estimated by the ratio between the incident (Pi) and the transmitted (Pt) power, as given in Eq. (8).

$$EMI\ SE = 10\log[\![Pi/Pt]\!] \tag{8}$$

Considering the propagation of an electromagnetic wave through an electrically conductive composite, two additional important parameters should be considered; the efficiency of the tested specimen in either absorb (SEA) or reflect (SER) the incident electromagnetic wave, described as:

$$SER = 10\log(1 - (S11)\text{^}2) \tag{9}$$

$$SEA = 10\log[\![(1 - (1 - (S11)\text{^}2 - (S21)\text{^}2)/(1 - (S11)\text{^}2)]\!] \tag{10}$$

2.3.6. Quasi-static tensile test

The uniaxial tensile tests were conducted on both, the extruded filaments and 3-D printed samples. Filaments specimens had a length of 150 mm, a gauge length of 100 mm and a diameter of 1.75 mm. The 3-D printed samples are described in Section 2.2.4. Tests were carried out at room temperature using an Instron® 5969 electromechanical tester (Norwood, MA, USA) equipped with a load cell of 50 kN. Yield and fracture properties were evaluated at a crosshead speed of 10 mm/min. The elastic modulus of 3D-printed samples was determined at a crosshead speed of 1 mm/min by an electrical extensometer Instron® model 2620-601 (Norwood, MA, USA) with a gage length of 12.5 mm. The elastic modulus of filaments with a gage length of 100 mm was tested at 10 mm/min. According to ISO 527 standard, the elastic modulus was determined as a secant value between strain levels of 0.05% and 0.25%. The reported results represent an average value of at least three replicates.

3. Results and discussion

3.1. Density measurements

Table 3 reports the densities of the carbonaceous fillers as well as the densities of neat ABS and the nanocomposites.

The density of neat ABS filament was found near 1.034 g/cm^3. Due to the addition of each type of filler, the densities of nanocomposites were increased to 1.048-1.051 g/cm^3. The specific gravity of neat ABS, informed by the supplier, was considered as the theoretical density of ABS and inputted into Eq. (2) to estimate the theoretical density of the composites. The density values of the additives, measured via helium pycnometry, were inserted into Eqs. (4) and (5) to calculate the volume fraction of each filler in the composites.

3.2. Rheological behavior

Rheological investigations provide insights about the filler dispersion in the matrix, network formation and the material's behavior during the process. Binary composites of ABS/CNT and ABS/CB were studied to better understand which formulations is the more promising to be employed for FDM application. The graphs given in Fig. 4 show the complex viscosity of ABS/CNT and ABS/CB as a function of frequency at 230 °C, for different amounts of filler content. It is possible to observe that the complex viscosity of ABS is already relatively high and increase with the addition of filler. At low frequencies, the viscosity increased by 2 orders of magnitude for ABS/CNT with 5 wt.% filler content and for ABS/CB with 10 wt.% filler content. The complex viscosity curves of ABS/CNT manifest a transition between 0.3 and 0.5 wt.% which indicates rheological percolation. For ABS/CB this transition is visible between 3 and 5 wt.%.

Because viscosity, for both CNT- and CB-based composites, increases highly between 3 and 5 wt.% a specific formulation of 3 wt.% of filler was chosen to continue the study and fabricate the FDM samples. Formulations at this weight fraction of fillers were considered the most appropriated for avoiding clogging the printing nozzle. Additionally, to choose a hybrid formulation, the same study was made. As it can be seen in Fig. 4, the complex viscosity showed by hybrid composites with different CNT/CB fractions, with a fixed total amount of filler (3 wt.%), increases with the increase of CNT. According to these results, a single formulation of ABS/CNT.CB with a total amount of 3 wt.% and a filler fraction of 50:50 has been selected to ensure an appropriate viscosity (Fig. 5).

3.3. Microstructure of the specimens obtained via FDM

In Fig. 6 both the photos of the FDM specimens as well as the micrographs of their fracture surfaces analyzed via optical microscopy are reported. The axes inserted into the images are in accordance with the

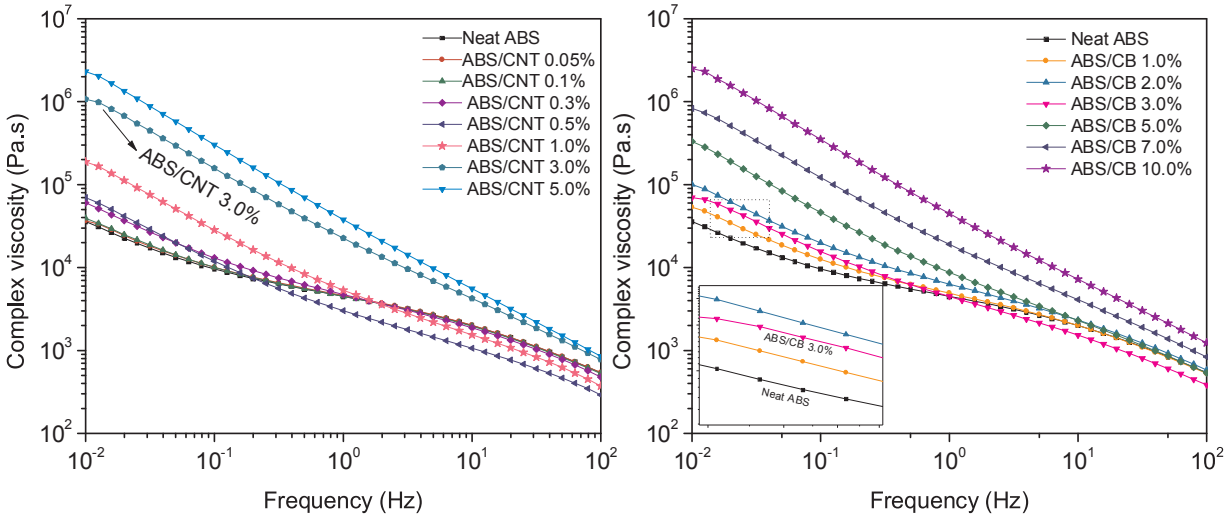

Fig. 4. Complex viscosity as a function of frequency for ABS/CNT and ABS/CB composites with various filler contents.

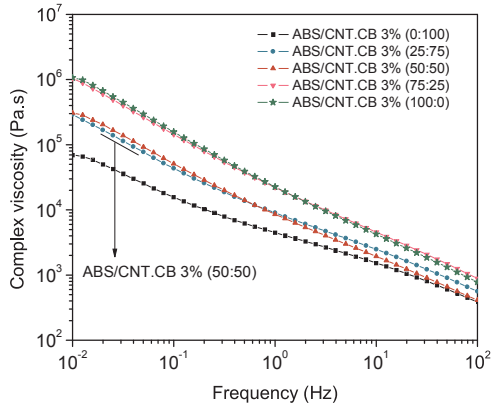

Fig. 5. Complex viscosity as a function of the frequency of ABS/HYB with 3 wt.% total filler amount at different fractions.

3D axis representation presented in Fig. 2. The photographs exhibit the FDM specimens of neat ABS and ABS/CNT for each growing direction.

The micrographs evidence the boundaries between the deposited filaments during the construction of the specimens. Since PC specimens were built perpendicularly to the collecting platform, in Fig. 6(b) the deposited filaments are forming the layer-upon-layer structure whereas for H45 and HC (Fig. 6(e) and (h), respectively) they were representative of the outermost surface.

Fig. 6(c) shows the top view at the left corner for PC specimen showing the presence of a central gap of 0.2 mm width (arrow inserted in the image) in the construction direction over the YX plane. The layer-upon-layer of H45 and HC are evidenced in the top view images of these specimens give in Fig. 6(f) and (i), respectively.

The images displayed in Fig. 7 are the cross-sections of the FDM specimens analyzed via SEM. For all the growing directions a reduction of the filament cross-section attributed to the cooling of the specimens and a possible orientation during FDM process can be observed. Similar shape modifications while processing via FDM have been already reported [6].

In addition, for PC specimens it is possible to see the central gap in the ZX plane and microvoids in the intersections of the filaments of respective layers. For H45 and HC, the images also revealed the presence of micro-voids between the filaments. In particular, for H45 in the direction of the filaments (Fig. 7(f)) the boundary formed by the deposited layers can be seen while for HC specimens the layers appear to be well compacted (Fig. 7(g)–(i)).

3.4. Electrical conductivity

The electrical conductivity values of the extruded filaments as a function of filler type are compared in Fig. 8. The electrical conductivity values of the nanocomposites were effectively modified in comparison to neat ABS due to the addition of carbonaceous fillers at the weight fraction 3 wt.%. The higher values were obtained for the composites with CNT followed by the hybrid systems and by the CB filled systems.

In particular, the electrical conductivity was significantly increased from about 10^{-15} S cm^{-1} of neat ABS up to 10^{-2} S cm^{-1} of ABS/CNT composites. ABS/CB composites showed the lowest electrical conductivity, around 10^{-7} S cm^{-1}. These differences can be attributed to CNT's higher aspect ratio, which facilitates the creation of a continuous conductive network within the ABS matrix. Moreover, CNTs are intrinsically more conductive than CB. When both CNT and CB were added to form the hybrid composites, the electrical conductive was found to be in the order of 10^{-3} S cm^{-1}. Therefore, CNT and CB together formed an efficient conductive network using half of the weight fraction of the carbon nanotube.

Fig. 9 shows the volume electrical conductivity of the specimens for each composite formulation as a function of the growing direction during FDM processing. Highlighting that the volume conductivity of FDM specimens was measured placing the terminals onto the opposites faces according to the 3-D axis representation given in Fig. 2: for PC plan YX; for HC and H45 plan ZX. According to Fig. 9, the volume conductivity of the specimens prepared via FDM was found to be dependent on their growing direction. Those built along PC direction manifest the highest volume conductivity values, nearly two orders of magnitude higher than HC and H45 growing directions independent on the composite formulation. For instance, in the case of ABS/CNT, the specimen built along PC direction had the volume conductivity measured near 10^{-6} S cm^{-1} whereas those specimens built along HC or H45 showed volume conductivity near 10^{-8} S cm^{-1}. Similar to ABS/HYB, the volume conductivity was found in the order of 10^{-7} for PC and 10^{-9} S cm^{-1} for HC and H45 growing directions.

The electrical conductivity of FDM specimens were approximately 5–6 orders of magnitude lower compared to the respective filament. It is assumed that the extruded filaments are homogeneous, do not present macro defects, and the fillers are adequately distributed and dispersed along the polymer matrix in a way that an efficient conductive network had been formed during extrusion. Therefore, the drop in the electrical conductivity is attributed to the change in printing patterns of the specimens manufactured via FDM and to the fact that a full compaction is not reached. In particular, the specimens built along PC

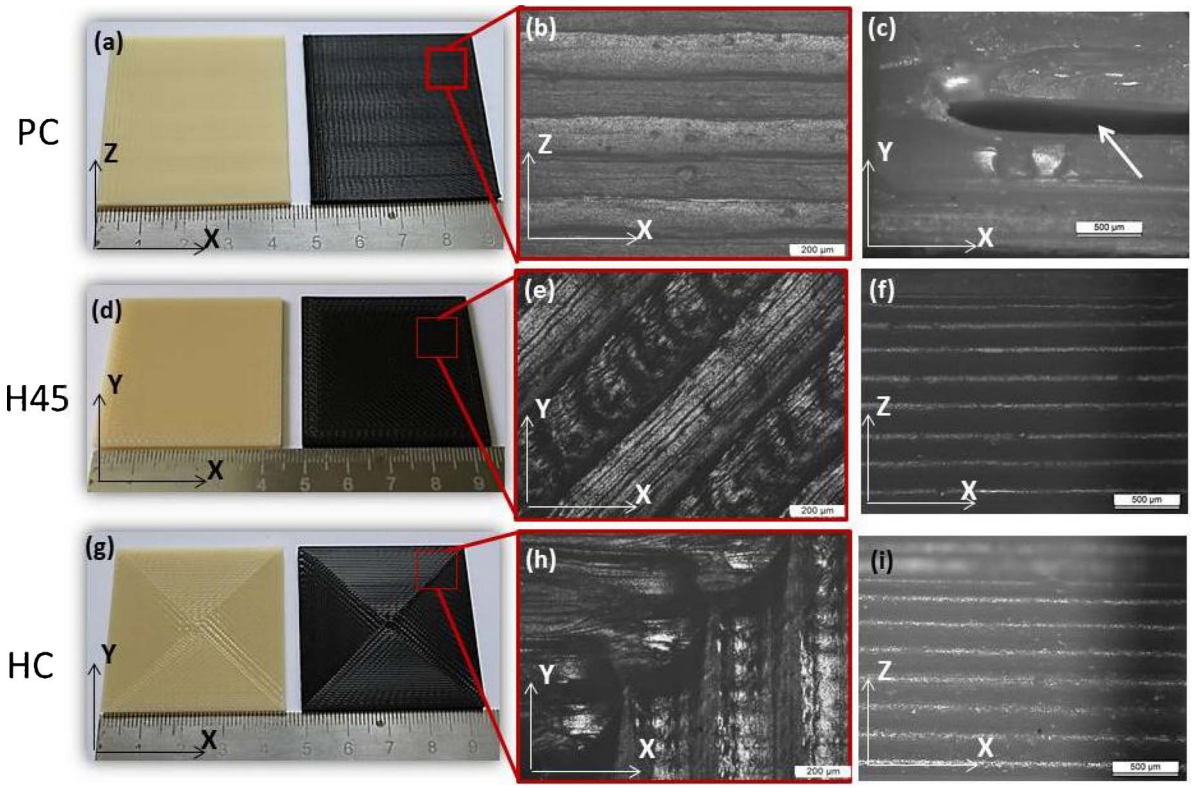

Fig. 6. Photographs of the FDM components: PC (a), H45 (d) and HC (g). Optical microscopy at 100 x magnification, PC (b), H45 (e) and HC (h). Optical microscopy at 50 x magnification top view of PC (c), H45 (f) and HC (i).

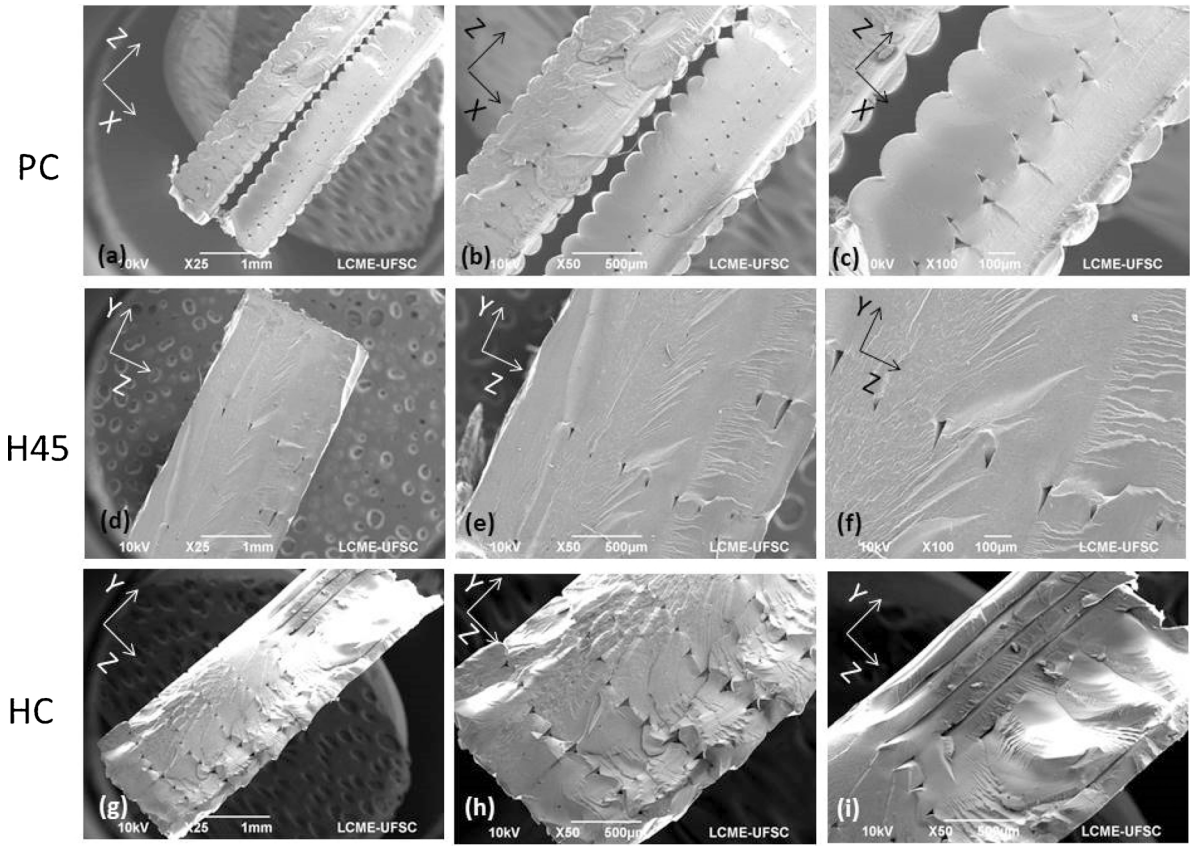

Fig. 7. SEM images of cross-section for respective growing directions: PC (a–c), HC (d–f) and H45 (g-h).

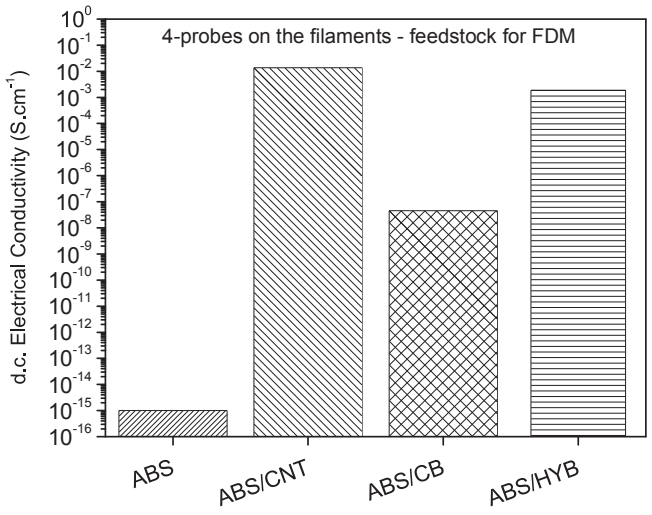

Fig. 8. D.C. electrical conductivity for the extruded filaments.

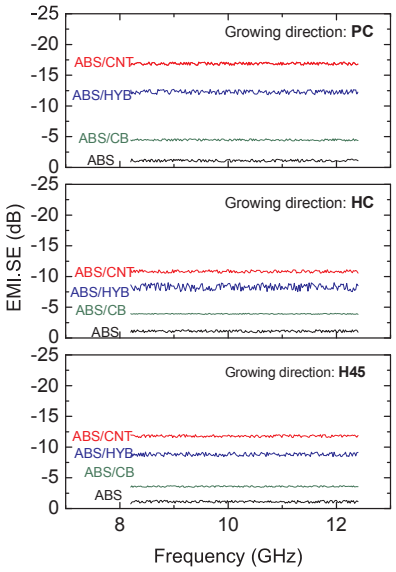

Fig. 10. Total electromagnetic interference shielding effectiveness of ABS carbon-based composites in three different layer-by-layer growing directions: perpendicular (upper graph), horizontal concentric (middle graph) and horizontal alternate (bottom graph).

direction have a more efficient conductive structure than HC and H45 specimens. The volume electrical conductivity of PC was approximately two orders of magnitude higher independent on the composite formulation, despite the fact that PC is approximately 0.40 g lighter and presented macro voids or holes along the body of the specimens. During the electrical conductivity tests, the electrical charges were offered less resistance as they were moved along the direction of the filaments, note that PC specimens present a continuous pathway, (see Fig. 6(c)). For H45 and HC instead, the electrical charges move throughout the specimens crossing the interfaces between the layers, lowering the volume conductivity of these specimens.

3.5. Electromagnetic interference shielding effectiveness

The stack plot given in Fig. 10 shows the total EMI SE for ABS composites specimens prepared via FDM as a function of their growing direction, recalling that the incident wave reached the respective faces of FDM specimens: for PC plan YX; for HC and H45 plan ZX, according to Fig. 2.

Accordingly, EMI SE responses were found to be a function of both the filler type as well as the growing direction of the specimens. Looking at the polymer composites formulations, the higher shielding effectiveness was achieved in the order following order: ABS/CNT > ABS/HYB > ABS/CB > neat ABS independent on the growing direction of the specimens.

Considering the printing patterns, it can be observed that the specimens prepared along the PC direction better attenuated the electromagnetic radiation. For instance, the total EMI SE of carbon nanotube-based composite built along PC was around −16 dB whereas the same composite built along HC and H45 showed an attenuation of −10 and −11 dB, respectively. Similar differences are observed for ABS/HYB, −12, −8 and −8 dB for PC, HC and H45 respectively. The ABS/CB showed lower values of attenuation, near −4 dB independent on the growing direction.

The shielding effectiveness is achieved by attenuating the power of the incident wave passing through the specimens wherein two main mechanisms are operating: the reflection or the absorption of the incident wave [18]. The two stack plots given in Fig. 11 make a distinction between both the shielding effectiveness by absorption (SEA) and shielding effectiveness by reflection (SER). It is possible to appreciate that absorption is the commanding mechanism of shielding when the incident wave propagates through the specimens.

The mechanisms of attenuation are a function of both the dielectric and the magnetic properties of the material to which the component is

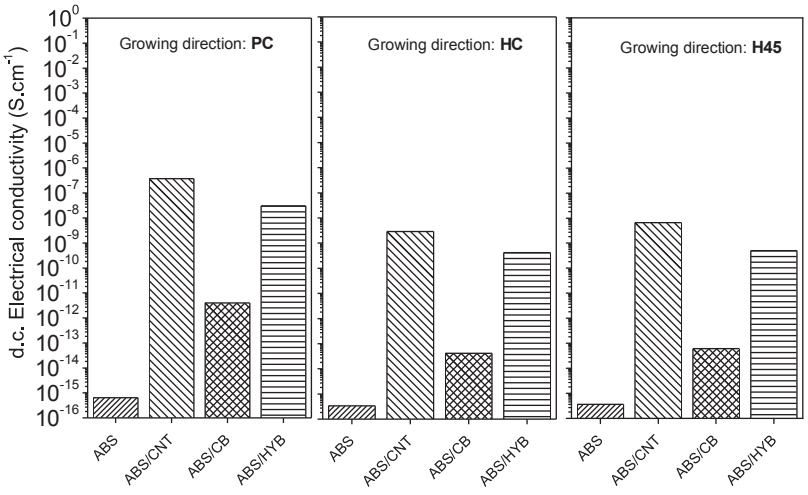

Fig. 9. D.C. volume conductivity of ABS carbon-based solid components produced via FDM in three different layer-by-layer growing directions: perpendicular (left graph), horizontal concentric (center graph) and horizontal alternate (right graph).

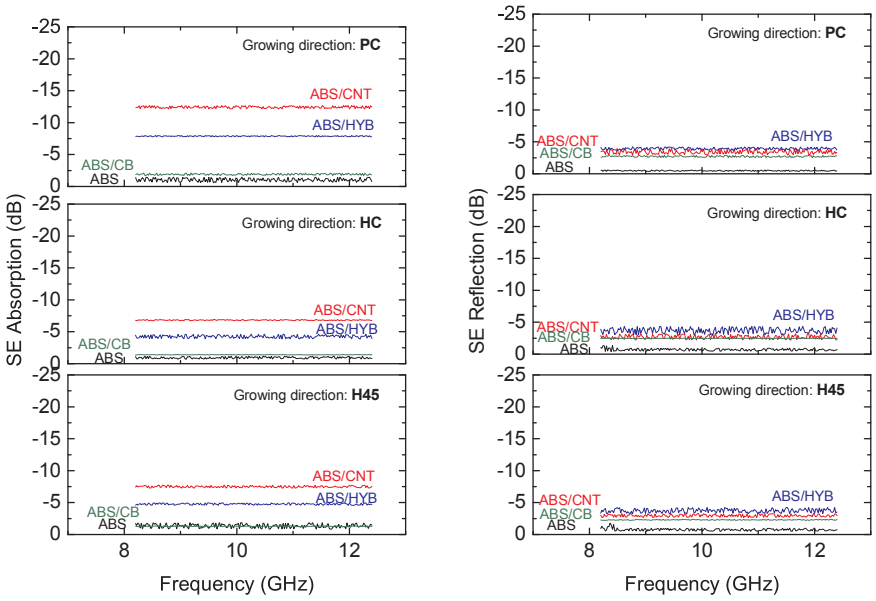

Fig. 11. Shielding by absorption (left stack plot) and by reflection portion (right stack plot) of ABS carbon-based composites in three different layer-by-layer growing directions: perpendicular (upper graph), horizontal concentric (middle graph) and horizontal alternate (bottom graph).

made of. Carbon-based composites are attributed changes at the electrical properties, i.e. dielectric constant, compared to neat matrix due to the addition of these fillers [19,28,29] and, therefore, the commanding attenuation by means of absorption is justified by the use of carbon-based fillers during the formulation of the ABS composites.

The outcomes of experimental measurements obtained in this work are displayed in Table 4. For obtaining 3-D components manufactured via FDM having high EMI SE responses, the first step is preparing the extruded feedstock filament with electrical conductivity as higher as possible, therefore, a proper selection of the filler and dispersion method is essential. In this work, the hybridization of CNT/CB reduced by half the weight fraction of carbon nanotubes and the extruded filaments of composites ABS/CNT and ABS/HYB showed similar electrical conductivity values. Nevertheless, once the 3-D components are manufactured the volume conductivity of the specimens seems to be a physical property that would indicate on EMI SE performances. The printing patterns should be designed in a way that the FDM manufactured component offers as low electrical resistance as possible to the movement of charges, i.e. higher volume electrical conductivity. In this work, the PC specimens, have shown the highest volume electrical conductivity, despite the presence of a lacuna, microvoids and reduced weight compared to the other growing directions. Consequently, the PC components have shown the highest EMI SE responses.

Materials for EMI shielding purposes are normally targeted to have a minimum of −20 dB of attenuation, at these values of shielding more than 99% of the incident wave is attenuated ensuring that electronic equipment does not generate, or is not affected by, electromagnetic interference [30,31]. The values of attenuation obtained in this work were lower than the minimum of attenuation that ensures safety. It is expected that formulations with a higher weight fraction of either CNT or a hybrid combination of CNT/CB could effortlessly go higher than −20 dB. For that, it would be necessary to overcome the limitation of processing high viscous composites formulations via FDM. Advanced machines that could work at higher deposition temperatures, lower deposition rate, and lower layer height could be a possible solution. On the other hand, it has been verified that components made of carbon-based ABS polymer composites manufactured via FDM can have their EMI SE optimized if appropriately designed and shaped.

3.6. Quasi-static tensile test

A tensile test was conducted on the extruded filaments as well as on the 3-D printed dumbbells at different growing orientations. The stress-strain curves of ABS and nanocomposites filaments are shown in Fig. 12. The influence of 3 wt.% of the carbonaceous fillers on the elastic modulus (E), strength (σ_{max}), and strain at break (ε_b) is described as follows: the addition of CNT and CB increased both the elastic modulus of the ABS matrix and its strength. The quasi-static tensile test conducted on the extruded filaments revealed higher elastic moduli, ca. 6–10%, due to the addition of CNT, CB, and CNT/CB. The strength of composites containing the amount 3 wt.% is increased from 45.1 MPa to 47.5 MPa (i.e. 5%), to 49.8 MPa (i.e. 10%) and to 49.6 MPa (i.e. 10%) for CB, CNT and CNT/CB nanofillers respectively.

The stress-strain curves of 3-D printed dumbbell specimens for each growing direction (PC, H45, and HC) are shown in Figs. 13–15, respectively. The mechanical properties reported are strongly dependent on the growing directions. The elastic modulus and strength of ABS/CNT, ABS/CB and ABS/HYB nanocomposites increase over unfilled ABS

Table 4
Electrical conductivity of extruded filament and the specimens obtained via FDM. Total EMI SE, shielding effectiveness by reflection (SER) and shielding effectiveness by absorption (SEA) at the frequency range of 8–12 GHz of neat ABS and carbon-based nanocomposites.

Composite formulation	σ of extruded filament (S cm^{-1})	Volume σ on FDM components (S cm^{-1})			EMI SE (dB)			SE Absorption (dB)			SE Reflection (dB)		
		PC	HC	H45	PC	HC	H45	PC	HC	H45	PC	HC	H45
ABS	10^{-16}	10^{-16}	10^{-16}	10^{-16}	1	1	1	< 1	< 1	< 1	< 1	< 1	< 1
ABS/CNT	10^{-2}	10^{-7}	10^{-9}	10^{-9}	16	10	11	12	7	7	4	3	4
ABS/CB	10^{-8}	10^{-14}	10^{-14}	10^{-14}	4	4	3	2	1	1	2	2	2
ABS/HYB	10^{-3}	10^{-8}	10^{-10}	10^{-10}	12	8	8	8	4	4	4	3	4

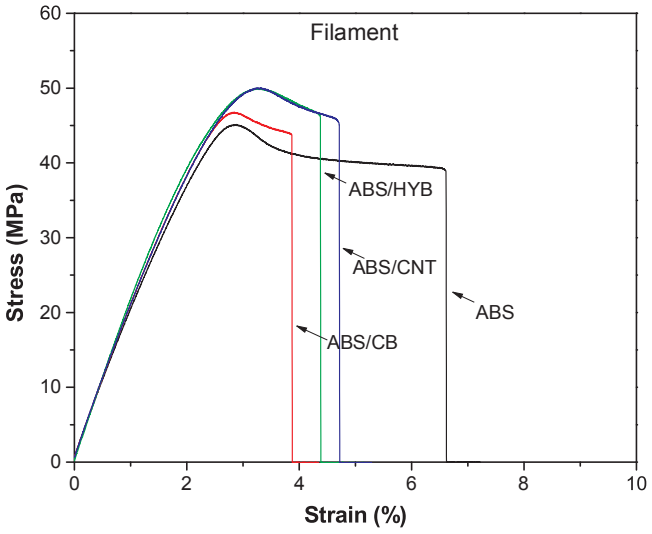

Fig. 12. Stress-strain curve of ABS and nanocomposites filaments.

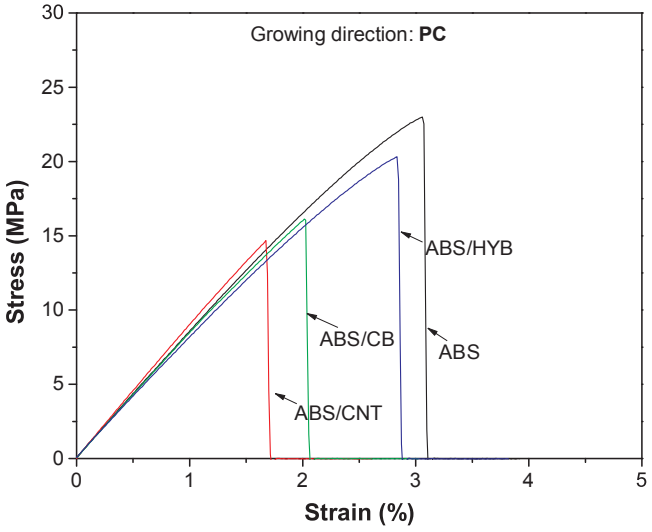

Fig. 13. Stress-strain curve of 3D-printed ABS and nanocomposites. Growing direction: PC.

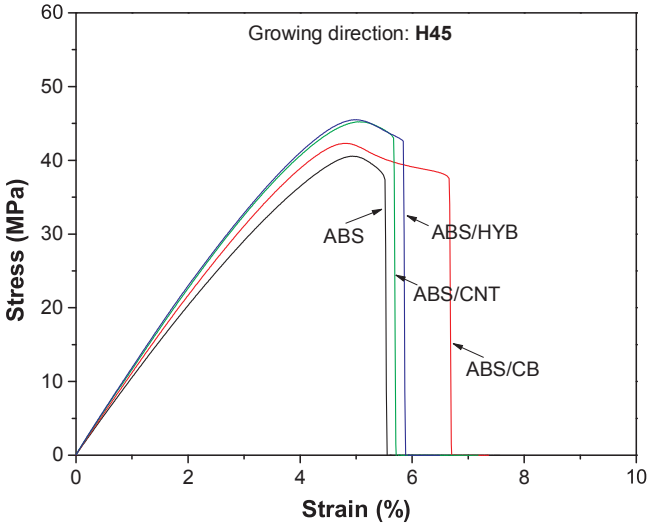

Fig. 14. Stress-strain curve of 3D-printed ABS and nanocomposites. Growing direction: H45.

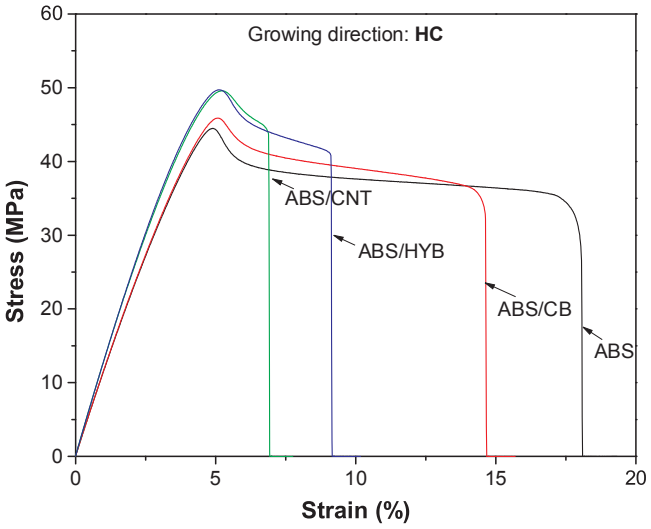

Fig. 15. Stress-strain curve of 3D-printed ABS and nanocomposites. Growing direction: HC.

for the two growing directions, HC and H45, the tensile modulus and strength of neat ABS printed at H45 and HC are comparable due to good contact between extruded filaments but the elongation at the break was substantially lower for H45 direction. These differences can be attributed to the internal orientations of deposited filaments. In particular, for the PC printed specimens, lower magnitudes for E and yield strength were detected attributed to the weakness of interlayer bonding and, for this growing direction, any influence attributed to the carbonaceous fillers on the investigated mechanical properties is difficult to be analyzed.

4. Conclusions

Multi-walled carbon nanotubes, carbon black and a 50:50 hybrid formulation were dispersed into ABS matrix at a fixed concentration of 3 wt.%. Extruded filaments of resulting polymer composites were prepared and used as feedstock for fused deposition modelling. The fused deposition modelling components were manufactured along three different printing orientations. The electrical conductivity, electromagnetic interference shielding efficiency and mechanical properties of resulting 3-D printed components were assessed.

The incorporation of carbonaceous filler in the ABS matrix resulted in an increase in complex viscosity. A fixed filler concentration of 3 wt. % has been selected for the preparation of the feedstock filaments for additive manufacturing of the specimens. At the weight fraction of 3%, the most appropriate correlation between the electrical conductivity and the viscosity of the composites had been observed.

Extruded filaments of the ABS loaded with 3 wt.% of multi-walled carbon nanotubes, carbon black and 50:50 hybrid composition have shown higher electrical conductivity values as well as improved mechanical properties such as elastic modulus and strength when compared to neat ABS.

The volume electrical conductivity, the electromagnetic interference shielding efficiency and the mechanical properties of 3D printed specimens are intensely dependent on the printing patterns

Acknowledgements

The work was supported by the Brazilian research foundation CNPq "*Conselho Nacional de Desenvolvimento Científico e Tecnológico*" - Brazil. Authors are grateful to the Central of Electron Microscopy Laboratory, Santa Catarina Federal University (LCME-UFSC), for the SEM analysis.

References

[1] L. Bade, P.M. Hackney, I. Shyha, M. Birkett, Investigation into the development of an additive manufacturing technique for the production of fibre composite products, Procedia Eng. 132 (2015) 86–93, http://dx.doi.org/10.1016/j.proeng.2015.12.483.

[2] J.W. Stansbury, M.J. Idacavage, 3D printing with polymers: challenges among expanding options and opportunities, Dent. Mater. 32 (2016) 54–64, http://dx.doi.org/10.1016/j.dental.2015.09.018.

[3] P. Parandoush, L. Tucker, C. Zhou, D. Lin, Laser assisted additive manufacturing of continuous fiber reinforced thermoplastic composites, Mater. Des. 131 (2017) 186–195, http://dx.doi.org/10.1016/j.matdes.2017.06.013.

[4] M. Mohsenizadeh, F. Gasbarri, M. Munther, A. Beheshti, K. Davami, Additively-manufactured lightweight Metamaterials for energy absorption, Mater. Des. 139 (2018) 521–530, http://dx.doi.org/10.1016/j.matdes.2017.11.037.

[5] F.S. Senatov, K.V. Niaza, A.I. Salimon, A.V. Maksimkin, S.D. Kaloshkin, Architected UHMWPE simulating trabecular bone tissue, Mater. Today Commun. 14 (2018) 124–127, http://dx.doi.org/10.1016/j.mtcomm.2018.01.001.

[6] S. Dul, L. Fambri, A. Pegoretti, Fused deposition modelling with ABS-graphene nanocomposites, Compos. Part A Appl. Sci. Manuf. 85 (2016) 181–191, http://dx.doi.org/10.1016/j.compositesa.2016.03.013.

[7] C. Balletti, M. Ballarin, F. Guerra, 3D printing: state of the art and future perspectives, J. Cult. Herit. 26 (2017) 172–182, http://dx.doi.org/10.1016/j.culher.2017.02.010.

[8] J.-Y.Y. Lee, J. An, C.K.K. Chua, Fundamentals and applications of 3D printing for novel materials, Appl. Mater. Today 7 (2017) 120–133, http://dx.doi.org/10.1016/j.apmt.2017.02.004.

[9] X. Tian, T. Liu, C. Yang, Q. Wang, D. Li, Interface and performance of 3D printed continuous carbon fiber reinforced PLA composites, Compos. Part A Appl. Sci. Manuf. 88 (2016) 198–205, http://dx.doi.org/10.1016/j.compositesa.2016.05.032.

[10] M. Kariz, M. Sernek, M. Obućina, M.K. Kuzman, Effect of wood content in FDM filament on properties of 3D printed parts, Mater. Today Commun. 14 (2018) 135–140, http://dx.doi.org/10.1016/j.mtcomm.2017.12.016.

[11] S. Berretta, R. Davies, Y.T.T. Shyng, Y. Wang, O. Ghita, Fused deposition modelling of high temperature polymers: exploring CNT PEEK composites, Polym. Test. 63 (2017) 251–262, http://dx.doi.org/10.1016/j.polymertesting.2017.08.024.

[12] J.W. Tseng, C.Y. Liu, Y.K. Yen, J. Belkner, T. Bremicker, B.H. Liu, T.J. Sun, A.B. Wang, Screw extrusion-based additive manufacturing of PEEK, Mater. Des. 140 (2018) 209–221, http://dx.doi.org/10.1016/j.matdes.2017.11.032.

[13] J.C.C. Riddick, M.A.A. Haile, R.V. Von Wahlde, D.P.P. Cole, O. Bamiduro, T.E.E. Johnson, Fractographic analysis of tensile failure of acrylonitrile-butadiene-styrene fabricated by fused deposition modeling, Addit. Manuf. 11 (2016) 49–59, http://dx.doi.org/10.1016/j.addma.2016.03.007.

[14] A. Dorigato, V. Moretti, S. Dul, S.H. Unterberger, A. Pegoretti, Electrically conductive nanocomposites for fused deposition modelling, Synth. Met. 226 (2017) 7–14, http://dx.doi.org/10.1016/j.synthmet.2017.01.009.

[15] C. Shemelya, A. De La Rosa, A.R. Torrado, K. Yu, J. Domanowski, P.J. Bonacuse, R.E. Martin, M. Juhasz, F. Hurwitz, R.B. Wicker, B. Conner, E. MacDonald, D.A. Roberson, Anisotropy of thermal conductivity in 3D printed polymer matrix composites for space based cube satellites, Addit. Manuf. 16 (2017) 186–196, http://dx.doi.org/10.1016/j.addma.2017.05.012.

[16] X. Wang, M. Jiang, Z. Zhou, J. Gou, D. Hui, 3D printing of polymer matrix composites: a review and prospective, Compos. Part B Eng. 110 (2017) 442–458, http://dx.doi.org/10.1016/j.compositesb.2016.11.034.

[17] S. Dul, Filaments production and fused deposition modelling of ABS/carbon nanotubes composites, Nanomaterials 8 (2018) 49, http://dx.doi.org/10.3390/nano8010049.

[18] J.M. Thomassin, C. Jérôme, T. Pardoen, C. Bailly, I. Huynen, C. Detrembleur, Polymer/carbon based composites as electromagnetic interference (EMI) shielding materials, Mater. Sci. Eng. R Rep. 74 (2013) 211–232, http://dx.doi.org/10.1016/j.mser.2013.06.001.

[19] S. Kashi, R.K. Gupta, T. Baum, N. Kao, S.N. Bhattacharya, Morphology, electromagnetic properties and electromagnetic interference shielding performance of poly lactide/graphene nanoplatelet nanocomposites, Mater. Des. 95 (2016) 119–126, http://dx.doi.org/10.1016/j.matdes.2016.01.086.

[20] D.D.L. Chung, Carbon materials for structural self-sensing, electromagnetic shielding and thermal interfacing, Carbon N. Y. 50 (2012) 3342–3353, http://dx.doi.org/10.1016/j.carbon.2012.01.031.

[21] L. Pourzahedi, P. Zhai, J.A.A. Isaacs, M.J.J. Eckelman, Life cycle energy benefits of carbon nanotubes for electromagnetic interference (EMI) shielding applications, J. Clean. Prod. 142 (2017) 1971–1978, http://dx.doi.org/10.1016/j.jclepro.2016.11.087.

[22] P. Verma, P. Saini, V. Choudhary, Designing of carbon nanotube/polymer composites using melt recirculation approach: effect of aspect ratio on mechanical, electrical and EMI shielding response, Mater. Des. 88 (2015) 269–277, http://dx.doi.org/10.1016/j.matdes.2015.08.156.

[23] A.H.A.H.A. Hoseini, M. Arjmand, U. Sundararaj, M. Trifkovic, Significance of interfacial interaction and agglomerates on electrical properties of polymer-carbon nanotube nanocomposites, Mater. Des. 125 (2017) 126–134, http://dx.doi.org/10.1016/j.matdes.2017.04.004.

[24] Y. Yang, M.C. Gupta, K.L. Dudley, Towards cost-efficient EMI shielding materials using carbon nanostructure-based nanocomposites, Nanotechnology 18 (2007) 345701, http://dx.doi.org/10.1088/0957-4484/18/34/345701.

[25] N. Joseph, C. Janardhanan, M.T. Sebastian, Electromagnetic interference shielding properties of butyl rubber-single walled carbon nanotube composites, Compos. Sci. Technol. 101 (2014) 139–144, http://dx.doi.org/10.1016/j.compscitech.2014.07.002.

[26] S. Kuester, C. Merlini, G.M.O. Barra, J.C. Ferreira, A. Lucas, A.C. De Souza, B.G. Soares, Processing and characterization of conductive composites based on poly(styrene-b-ethylene-ran-butylene-b-styrene) (SEBS) and carbon additives: a comparative study of expanded graphite and carbon black, Compos. Part B Eng. 84 (2016) 236–247, http://dx.doi.org/10.1016/j.compositesb.2015.09.001.

[27] K. Gnanasekaran, T. Heijmans, S. van Bennekom, H. Woldhuis, S. Wijnia, G. de With, H. Friedrich, 3D printing of CNT- and graphene-based conductive polymer nanocomposites by fused deposition modeling, Appl. Mater. Today 9 (2017) 21–28, http://dx.doi.org/10.1016/j.apmt.2017.04.003.

[28] Y. Li, B. Shen, D. Yi, L. Zhang, W. Zhai, X. Wei, W. Zheng, The influence of gradient and sandwich configurations on the electromagnetic interference shielding performance of multilayered thermoplastic polyurethane/graphene composite foams, Compos. Sci. Technol. 138 (2017) 209–216, http://dx.doi.org/10.1016/j.compscitech.2016.12.002.

[29] S.E.E. Zakiyan, H. Azizi, I. Ghasemi, Influence of chain mobility on rheological, dielectric and electromagnetic interference shielding properties of poly methyl-methacrylate composites filled with graphene and carbon nanotube, Compos. Sci. Technol. 142 (2017) 10–19, http://dx.doi.org/10.1016/j.compscitech.2017.01.025.

[30] S.D.A.S. Ramôa, G.M.O. Barra, C. Merlini, W.H. Schreiner, S. Livi, B.G. Soares, Production of montmorillonite/polypyrrole nanocomposites through in situ oxidative polymerization of pyrrole: effect of anionic and cationic surfactants on structure and properties, Appl. Clay Sci. 104 (2015) 160–167, http://dx.doi.org/10.1016/j.clay.2014.11.026.

[31] B.G. Soares, M.E. Leyva, G.M.O. Barra, D. Khastgir, Dielectric behavior of polyaniline synthesized by different techniques, Eur. Polym. J. 42 (2006) 676–686, http://dx.doi.org/10.1016/j.eurpolymj.2005.08.013.